Plasma Rotation and Transport in the MAST Spherical Tokamak

[1]A. R. Field, [1]C. Michael, [1]R. J. Akers, [2]J. Candy, [1, 3]G. Colyer, [4]W. Guttenfelder, [3]Y.-c. Ghim(Kim), [1]C. M. Roach, [1]S. Saarelma and the MAST team.

[1]EURATOM/CCFE Fusion Association, Culham Science Centre, Abingdon, Oxon, UK.
[2]General Atomics, P.O. Box 85608, San Diego, CA 92186-5608, USA.
[3]Rudolf Peierls Centre for Theoretical Physics, University of Oxford, Oxford, UK.
[4]Princeton Plasma Physics Laboratory, P.O. Box 451, Princeton, NJ, USA.

E-mail: Anthony.field@ccfe.ac.uk

Abstract: The formation of internal transport barriers (ITBs) is investigated in MAST spherical tokamak (ST) plasmas. The roles of E×B flow shear, q-profile (magnetic shear) and MHD activity in their formation and evolution are studied using data from high-resolution kinetic- and q-profile diagnostics. In L-mode plasmas, with co-current directed NBI heating, ITBs in the momentum and ion thermal channels form in the negative shear region just inside q_{min}. In the ITB region the anomalous ion thermal transport is suppressed, with ion thermal transport close to the neo-classical level, although the electron transport remains anomalous. Linear stability analysis with the gyro-kinetic code GS2 shows that all electrostatic micro-instabilities are stable in the negative magnetic shear region in the core, both with and without flow shear. Outside the ITB, in the region of positive magnetic shear and relatively weak flow shear, electrostatic micro-instabilities become unstable over a wide range of wave-numbers. At ITG length scales, flow shear reduces linear growth rates and narrows the spectrum of unstable modes, but flow shear suppression of ITG modes is incomplete. Flow shear has little impact on growth rates at ETG scales. This is consistent with the observed anomalous electron and ion transport in this region. With counter-NBI ITBs of greater radial extent form outside q_{min} due to the broader profile of E×B flow shear produced by the greater prompt fast-ion loss torque.

1. Introduction

Shear-flow suppression of anomalous turbulent transport plays an important role in determining the confinement properties of spherical tokamak plasmas. In MAST the strong toroidal rotation, with typical Mach number $M_\phi = R\omega_\phi / v_{th,i} \leq 0.5$ (where ω_ϕ is the rotation rate and $v_{th,i}$ the ion thermal velocity), driven by tangential neutral beam injection (NBI) heating produces E×B shearing rates sufficient to exceed the growth rate of low-k ion-scale turbulence. In H-mode plasmas ion heat transport is within a factor 1-3 of the ion neo-classical level over most of the radius, while the electron transport remains highly anomalous [1, 2]. In L-mode plasmas however the ion transport can significantly exceed neo-classical levels in the outer regions but is suppressed by flow shear at mid-radius and, under favorable conditions can exhibit an internal transport barrier (ITB) with ion transport at the neo-classical level. Studies of transport in such regimes in MAST are facilitated by the availability of advanced diagnostics, including a high-resolution, multi-pulse NdYAG Thomson scattering system with resolution (~ 1 cm) matching that of the CXRS system and a multi-channel Motional Stark Effect (MSE) diagnostic for q-profile measurements. The integrated analysis chain (MC^3) used to prepare data for transport analysis using TRANSP [3] now incorporates the MSE constrained EFIT equilibrium reconstruction, allowing local transport properties to be related to details of the q-profile evolution.

An Internal Transport Barrier (ITB) can be defined as a region of reduced anomalous transport in the plasma core, associated with strong E×B flow shear, low or negative magnetic shear $\hat{s} = r/q \cdot (dq/dr)$ and a suppression of turbulence. In several tokamaks ITB formation is observed to be linked to low-order rational surfaces, where the transport improvement is initiated or tied to locations with rational q-values. In many cases the ITB is initiated when the location of zero magnetic shear ($q_{\min}$) passes through an integer value. Two mechanisms

proposed for ITB formation are related to coherent MHD modes and to the density of rational surfaces respectively. In the first [4, 5] tearing modes or fast-particle driven 'fishbone' modes are thought to modify the radial electric field (E_r) profile and hence trigger the ITB through increased E×B flow shear suppression of the turbulence. The second relies on the rarefaction of low-order rational surfaces in the vicinity of integer q-values [6, 7], which could lead to decreased coupling between micro-instabilities. In regions of negative magnetic shear, growth rates of micro-instabilities are also reduced due to a reduction in the interchange drive [8, 9].

The phenomenology of MAST discharges exhibiting ITBs, heated with both co- and counter NBI heating, is presented in Sect. 2, including results of local transport analysis. The location and time of ITB formation is shown to be related to the q-profile evolution, and the role of MHD activity in limiting the sustainment and in the termination of the ITB is discussed. In Sect. 3 results of micro-stability analysis of the co-NBI ITB discharge are presented both from the linear gyro-kinetic flux-tube code GS2, which incorporates flow shear [10], and also with the global, particle in cell (PIC) code ORB5 [11]. These analyses reveal the importance of flow shear and magnetic shear to micro-stability and hence to the level of anomalous transport.

2. ITB discharges

In DIII-D [12], discharges exhibiting transport changes at rational q values are low-density, L-mode discharges with NBI heating power marginal for ITB formation applied early to produce negative magnetic shear in the plasma core. Steepening in gradients of T_i and toroidal rotation ω_ϕ is observed as $q_{\min}$ passes through integer values, with a simultaneous reduction in low-k turbulence observed with the BES diagnostic. On JET [4], ITBs have also been linked to integer q values, forming when $q_{\min}$ reaches an integer value and then bifurcating, propagating both inwards and outwards with foot points following the two integer q surfaces. In NSTX [13] ITBs in the ion thermal and momentum channels are observed to form in the vicinity of maximum E×B shear, consistent with the E×B shear stabilization of ITG turbulence, while electron ITBs are more closely correlated with the region of most negative magnetic shear.

The ITB scenario used on MAST is similar to that of other tokamaks [14, 15], with early NBI heating of a low-density L-mode discharge applied during the current ramp to slow current penetration, resulting in strong toroidal rotation and reversed

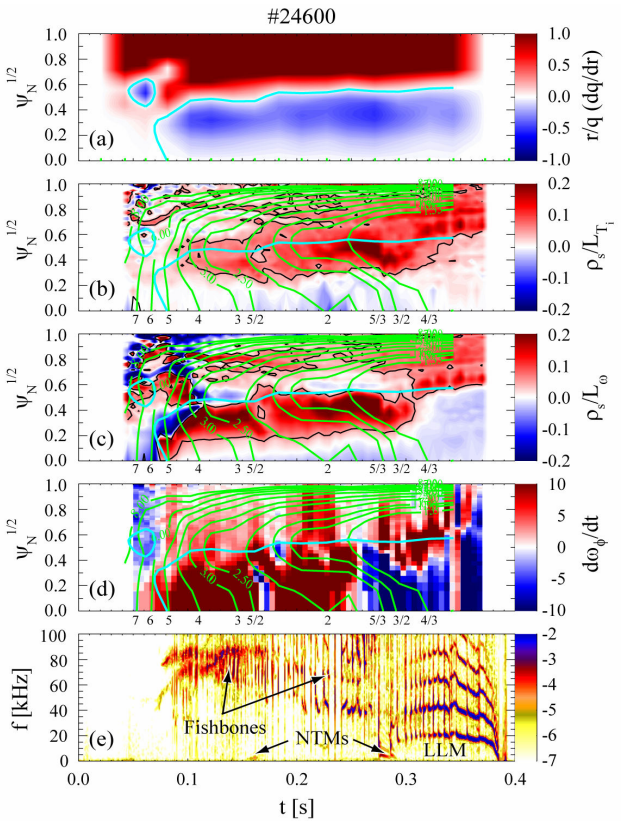

Fig. 1 Evolution of (a) magnetic shear $\hat{s}$, (b) normalised ion temperature ρ_s/L_{T_i} and (c) toroidal rotation ρ_s/L_ω gradients, (d) rate of change of toroidal rotation $\dot{\omega}_\phi$ and (e) MHD in co-NBI ITB discharge #24600. Locations of rational surfaces (green, labled below plots) and q_{min} (cyan) are also shown.

magnetic shear in the core. One aim is to investigate the relative importance of rotation shear compared to magnetic shear by comparing discharges with co- and counter-NBI heating in which the ratio of power to torque is different.

Co-NBI discharge:

The evolution of such an ITB discharge with ~ 3 MW of co-NBI heating (I_p ~ 850 kA, B_t ~ 0.53 T) is shown in Fig. 1. The ITB in the ion thermal channel forms at about 0.1 s when the ion thermal diffusivity χ_i locally falls to the ion neo-classical value. At this time the core T_i is only about 300 eV, although the normalised ion temperature gradient ρ_s/L_{T_i} (where ρ_s is the ion Larmor radius at the sound speed and $L_{T_i} = (T_i'/T_i)^{-1}$) already reaches 0.1. The ITB forms in the negative shear region just inside $q_{\min}$ about the time at which $q_{\min}$ reaches 3. An ITB in the momentum channel forms before this, at the onset of negative magnetic shear at ~ 0.07 s, with a peak in ρ_s/L_ω localised to the region of most negative magnetic shear a few cm inside $q_{\min}$. This is stronger than the ion thermal ITB with the maximum of ρ_s/L_ω ~ 0.2 located inside the peak of ρ_s/L_{T_i}. There is no sign of ITB formation in the electron channel, as the T_e profile is broad with the gradient distributed over the full radial region outside $q_{\min}$.

The formation of the ITB is better illustrated in Fig. 2, which shows the evolution of the maxima of ρ_s/L_{T_i} and ρ_s/L_{ω_ϕ} and their radial locations, which are close to that of $q_{\min}$. The times when $q_{\min}$ reaches rational values are also indicated. These times show some correlation with temporary increases in ρ_s/L_{ω_ϕ} and temporary reductions in ρ_s/L_{T_i}, which increases in the periods between the integer-q crossings. Such behaviour has also been observed on DIII-D [12].

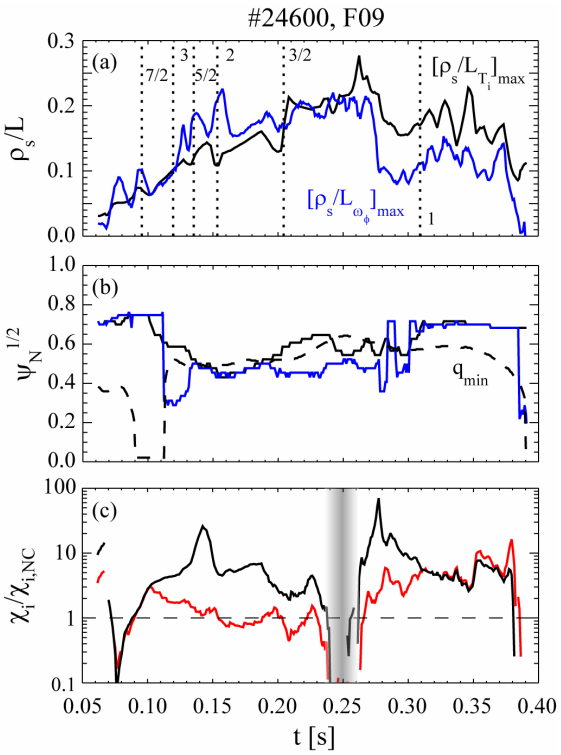

Fig. 2 Evolution of: (a) the maximum values of ρ_s/L_{T_i} (black), ρ_s/L_{ω_ϕ} (blue) and (b) their radial locations along with that of q_{min} (dashed) and (c) the ratio $\chi_i/\chi_{i,NC}$ at the location of $(\rho_s/L_{T_i})_{\max}$ (red) and at r/a = 0.7 (black) for the discharge shown in Fig. 1. Times when q_{min} crosses rational values are also shown in (a).

Thermal transport analysis requires knowledge of the heating profiles. The deposition of the dominant NBI heating is determined in TRANSP [3] using the NUBEAM Monte-Carlo model, which assumes classical behaviour of the fast-ions. Several factors indicate that, under some conditions, the loss rate of fast-ions must exceed that due to classical diffusion, primarily due fast-ion driven MHD activity. Firstly, the plasma energy W_{MHD}^{EFIT} estimated from EFIT is much lower than that calculated by TRANSP. In discharge #24600 in the period with two beams, TRANSP overestimates W_{MHD} by a factor ≤ 1.7 compared to EFIT. Overestimating the total pressure results a predicted Safranov shift ΔR_{Sh} that is ≤ 5 cm larger than the value obtained from EFIT. A further consequence is that the predicted D-D neutron rate R_N is a factor ≤ 2 too high compared to that measured.

Anomalous fast-ion losses can be represented in TRANSP using a diffusion coefficient D_{fast} which is isotropic in pitch angle, with prescribed radial and energy dependencies. It is necessary to assume anomalous losses in discharge #24600 only after 0.21 s when the NBI power is increased from ~ 1.8 MW to

~ 3.2 MW, indicating a strong power dependence of the losses. In this phase a value of D_{fast} ~ 3 m^2s^{-1} is required and after 0.27 s, following the onset of an n = 1 internal kink mode in the core, an even higher value ~ 5 m^2s^{-1} has to be assumed. Anomalous diffusion is applied only to fast-ions with energies > 30 keV, which is necessary to reduce R_N by a larger factor than W_{MHD}, as the D-D fusion cross-section is strongly weighted to higher energies. The enhanced fast-ion losses result in the absorbed power being reduced by factors of ~ 0.4 and ~ 0.5 in these two latter phases respectively.

With these assumptions on the fast-ion losses, as shown in Fig. 2 (c), the inferred level of ion thermal transport at the ITB location is close to the neo-classical value with $\chi_i/\chi_{i,NC}$ ~ 1, whereas χ_i considerably exceeds the neo-classical value in the positive shear region outside $q_{\min}$, e.g. by an order of magnitude at r/a ~ 0.7. In the latter phase (> 0.21s) with two beams, there is a period (0.24-0.27 s) exhibiting negative values of q_i and hence χ_i (indicated by the shaded region). This occurs because the magnitude of q_i is relatively small and hence sensitive to systematic uncertainties in the power deposition profile, which is dependent on the crude ad-hoc fast-ion redistribution model, and to rapid changes in the kinetic energy $\dot{W}_{kin}$ at this time.

During the period from 0.07-0.16 s, during which the ITB forms, there is strong 'fishbone' MHD activity driven by the fast-ion pressure gradient, localised around $q_{\min}$. At this time the rotation exhibits an inverted (positive) gradient just outside $q_{\min}$ indicating the presence of a localised negative torque there. Such a torque would arise from an outward redistribution of the fast-ions by the fishbone MHD activity, which would be balanced by an inward radial return current resulting in a $j_r \times B_\theta$ torque counter to I_p. Although this braking reduces ρ_s/L_ω at $q_{\min}$, it enhances the rotation gradient just inside $q_{\min}$ in the region of favourable negative magnetic shear, hence locally increasing the E×B shearing rate γ_E, which is proportional to L_ω^{-1}. This process may therefore facilitate formation of the ITB and perhaps also help localise it to the region inside $q_{\min}$.

Once the ITB is established T_i and ω_ϕ both increase rapidly inside $q_{\min}$, which is located at about r/a ~ 0.5, with T_i increasing to 2.5 keV and ω_ϕ to 2×10^5 s^{-1} on axis, while T_e reaches 1.5 keV. This rotation rate corresponds to a Mach number M_ϕ ~ 0.5. The stored energy W_{pl} reaches 100 kJ, including that of the fast-ions, which is comparable to the thermal energy. The strong pressure gradient at the ITB causes growth of NTM instabilities. Such a mode is observed in the discharge in Fig. 1 at about 0.16 s, which causes a localised braking of rotation inside $q_{\min}$ and an acceleration further outside, due to coupling with another mode of different mode number. This weakens the gradients, causing the mode to die away and the ITB to be sustained. Another tearing mode occurs later in the discharge at 0.28 s, which causes a similar localised braking of the core rotation. An example of such coupling of n = 3 and n = 2 tearing modes at q = 4/3 and 3/2 surfaces respectively is shown in Fig. 3, where the three independent measurements are all consistent. Although the ITB terminates around this time the tearing mode is not the sole cause. Once the central q_0 approaches unity at about 0.25 s, the plasma core becomes unstable to an internal n = 1, m = 1 internal kink mode, localised to the region where q < 1, which subsequently grows in

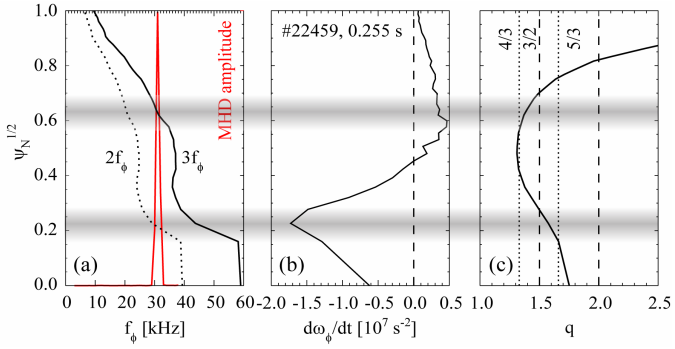

Fig. 3 Example of coupling of n= 3 mode at q = 4/3 surface to n= 2 mode at q = 3/2 showing: (a) n×ω_ϕ and MHD spectrum, (b) torque ∝ dω_ϕ/dt, (c) q-profile.

amplitude and saturates [16]. The resulting axially asymmetric perturbation causes braking of the core rotation due to neo-classical toroidal viscocity (NTV) [17]. This flattens the rotation profile inside the $q = 1$ surface and leads to termination of the ITB within about 30 ms. Such modes, which are referred to as Long-Lived Modes (LLM) usually occur in MAST plasmas once q_0 falls below ~ 1.3.

Counter-NBI discharge:

Heating by counter-current directed NBI is less efficient due to higher level of first-orbit losses of the fast ions. The beam torque however is of similar magnitude for a given injected power P_{inj} because of the increased co-beam directed $j_r \times B$ torque produced by the return current which balances the loss of fast-ions. Typically, the fraction of P_{inj} absorbed by the plasma is ~ 0.5 compared to over ~ 0.8 for co-injection, while the beam torque ~ 1 Nm is comparable. The rotation rate achieved is therefore similar to that with co-NBI. Perhaps surprisingly, the peak stored energy W_{MHD} ~ 80 kJ is not greatly reduced compared to the similar co-NBI discharge (shown in Fig. 1), hence the confinement with counter-NBI is improved. The temperatures in the counter-discharges are however lower with $T_i \leq 800$ eV and $T_e \leq 600$ eV and the profiles broader. Although the fuelling rates are comparable increased particle confinement with counter-NBI leads to a factor ~ 2 higher density. As in the co-discharge, the magnetic shear is weakly negative in the core inside $r/a \sim 0.4$.

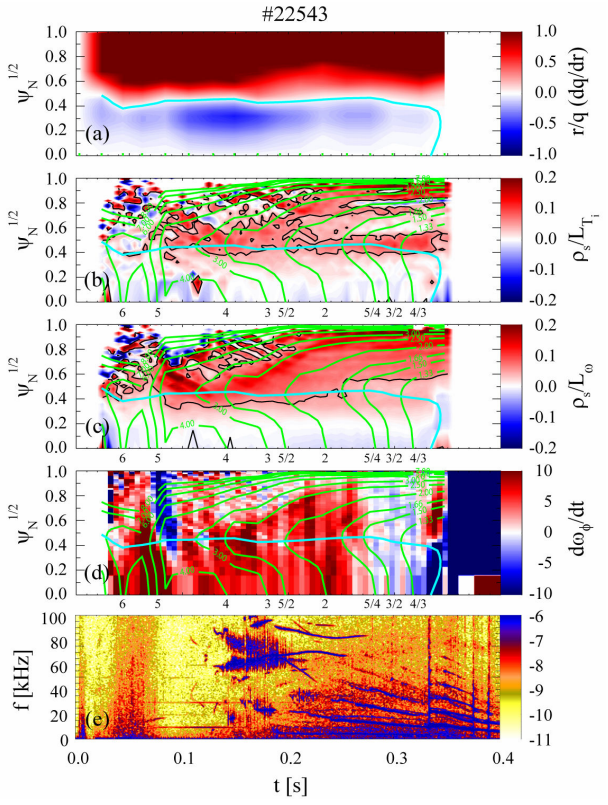

Fig. 4 Evolution of a counter-NBI ITB discharge #22543 with plots as defined in Fig. 1.

An ITB forms in the momentum channel at about 0.07 s (see Fig. 4). This can be seen as an acceleration of the core plasma inside $q_{\min}$ and a braking outside. The ITB forms just outside $q_{\min}$ at about r/a ~ 0.5 in the region of $\hat{s} > 0$ and the rotation gradient then broadens across the whole outer region of the plasma. This is consistent with the broad profile of $j_r \times B$ torque from the beams. The T_i gradient also increases at the same time at the same location outside $q_{\min}$, although the ITB is weaker with ρ_s / L_{T_i} ~ 0.1. After $q_{\min}$ falls below 5/2, the ion ITB appears to bifurcate with a second ITB at larger radius following the approximate location of the $q = 5/2$ surface. Across most of the plasma radius χ_i is within a factor ~ 2 of the ion neo-classical value while χ_e is several times larger. The assumption of anomalous fast-ion losses is not required in these counter-NBI discharges to match W_{MHD} and R_N.

3. Simulations

It is well known that radially sheared equilibrium flows $\boldsymbol{V}$ can suppress turbulence if the E×B shearing rate γ_E is larger than the maximum linear growth rate $\gamma_{\max}$ [18], i.e. $\gamma_E = dV_\perp / dr > \gamma_{\max}$. ITG turbulence can be affected when $\gamma_E \sim \mathrm{O}(v_{th,i}/L)$, where L is an equilibrium scale length. Equilibrium flows which approach sonic speeds are toroidal as the

poloidal component generated by E_r is cancelled by the parallel neo-classical flow. Sheared toroidal equilibrium flow $V = R\omega(\psi)\mathbf{e}_\phi$ has been implemented in the local, flux-tube geometry, gyro-kinetic code GS2 [19] in the intermediate flow ordering, where $v_{th,i} >> V >> (\rho_i/L)v_{th,i}$ [10]. Sheared flows introduce two additional physics terms into the gyro-kinetic equation. The perpendicular component γ_E tears apart radially extended eddies and is generally stabilising, while the parallel component $\sim(B_\phi/B_\theta)\gamma_E$ drives the parallel velocity gradient driven instability [20] and can enhance the growth rate of ITG modes [21]. The ratio of turbulence suppression to additional drive is proportional to $(B_\theta/B_\phi)\sim r/(Rq)$, i.e. suppression is favoured at low q and at large r/R, which arise by definition in an ST.

Nonlinear simulations for the conventional aspect ratio Cyclone base case equilibrium have demonstrated that the sheared parallel component of the flow can rekindle turbulence at large sheared flow [10, 22, 23]. This analysis has recently been extended to study turbulent toroidal momentum transport, and to assess the detailed sensitivity of turbulent fluxes to ρ_s/L_{T_i} and γ_E [24, 25]. At high values of sheared flow or low magnetic shear, the sheared parallel flow transiently drives instability growth, which can support sub-critical turbulence observed in recent simulations [24, 25, 26]. Furthermore, a possible physics mechanism, through which plasma equilibria may bifurcate to ITB profiles with steeper gradients, has been found to be more effective when the magnetic shear is zero rather than finite [25]. These results may be relevant to ITB formation in MAST.

A procedure to determine effective linear growth rates in local linear gyro-kinetic simulations with flow shear was outlined in [10]. In previous work [10, 27], local linear electrostatic analyses were performed at close to mid-radius ($\rho_n(=\Phi_N^{1/2}) = 0.4$, where Φ_N is the normalised toroidal flux) for the MAST H-mode plasma #6252. The trapped particle drives for low-k modes ($k_y\rho_i < \mathrm{O}(1)$) were shown to be weak owing to collisions, and the flow shear was found to be sufficient to stabilise all linear, low-k electrostatic instabilities in this region [10].

A similar linear analysis has been performed for the co-NBI ITB discharge #22807 (which is similar to #24600 shown in Fig. 1) at the time of peak ITB strength (0.25 s) at three radial locations of ρ_N = 0.3, 0.52 and 0.7, which are located inside the ITB region, just outside $q_{\min}$ and in the outer region of the plasma. At the innermost location where $\hat{s} < 0$, the linear electrostatic analysis shows that all modes at both ion and electron scales are stable with or without flow shear. Including magnetic perturbations without sheared flow did not change this result. Further calculations are underway to determine whether the core region is also fully stable at earlier times prior to the ITB formation. Fig. 5 (a, b) shows that at mid-radius, just outside $q_{\min}$ where $\hat{s}$ is slightly positive, it is important to include kinetic electron

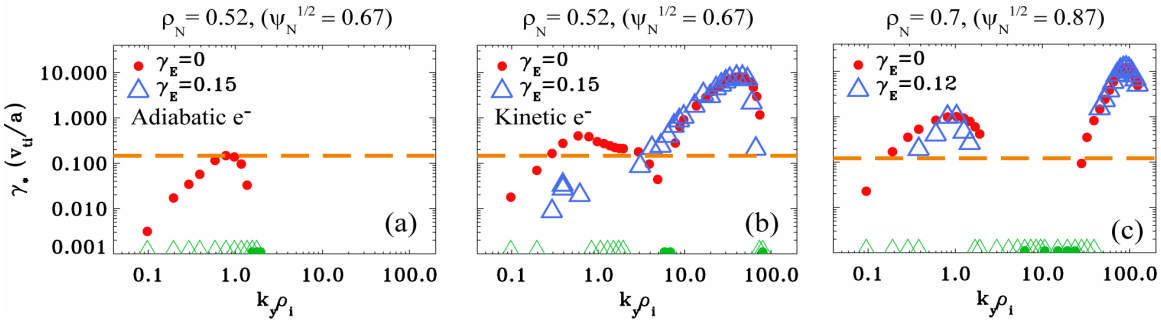

Fig. 5: Effective linear growth rate γ_* vs. perpendicular wave-number $k_y\rho_i$ with (triangles) and without sheared equilibrium toroidal flow (circles) for co-NBI ITB discharge #22807 (0.25 s) at (a, b) mid-radius and (c) in the outer region. Simulations were carried out with: (a) kinetic ions and adiabatic electrons and (b, c) with kinetic electrons and ions. The horizontal dashed lines show the local level of flow shear γ_E and symbols at the axis minimum denote stable modes.

physics because there is an appreciable trapped electron drive for TEM modes ($k_y\rho_i < \mathrm{O}(1)$) there. It is important to note that the collisionality is lower and the density gradient higher than in the H-mode equilibrium discussed in Refs. 10 and 27.

Including flow shear and kinetic electrons results in substantial but incomplete suppression of these low-*k* instabilities (Fig. 5 (b)), but without including a kinetic drive from trapped electrons, the ITG modes would be fully stabilised by the flow shear (Fig. 5(a)). On the outermost surface, a stable gap appears in the spectral range between the ITG and ETG regions: i.e. the TEM modes are stable because the plasma is more collisional. Strongly growing ITG modes ($k_y\rho_i < \mathrm{O}(1)$) are not fully stabilized by the weak flow shear in this outer region. Anomalous thermal and momentum transport is hence to be expected in this region, which is consistent with observations (see Fig. 2 (c)). Doubling the flow shear would be sufficient to fully suppress the ITG modes here. In summary, these calculations indicate that flow shear is not required to sustain the ITB in the negative shear core region but that it is acting to reduce the level of transport due to low-*k* TEM modes at mid-radius. The outer region is, however, unstable to ITG modes at the prevailing level of flow shear, which would result in anomalous ion heat transport.

The linear stability to ITG modes of discharge #22807 at 0.25s when the ITB is strongest has also been analysed using the global electrostatic code ORB5 [28, 11] and the local version of GYRO [29]at the most unstable location (ρ_N = 0.52). The results of these calculations are consistent with the GS2 analysis.

In the event where low-*k*, ion scale micro-instabilities are present, global, non-linear simulations are required to capture equilibrium variation over the large domain required for the simulation. This has motivated modelling of the ITG turbulence in this ITB discharge using ORB5 [11]. Simplified, non-linear ITG simulations without flow shear and with adiabatic electrons, show that the turbulence spreads inwards from the linearly unstable outer region to the stable inner region. With the experimental T_i gradient, the ion heat flux q_i saturates at just below the neo-classical level. As shown in Fig. 6, modest increases in the gradient result in considerably increased transport indicating that ITG turbulence may be clamping the T_i profiles, i.e. that the ion transport is stiff in the region outside the ITB. Global simulations with both sheared equilibrium flow and kinetic electrons are clearly required to capture fully the dynamics of the ion scale turbulence.

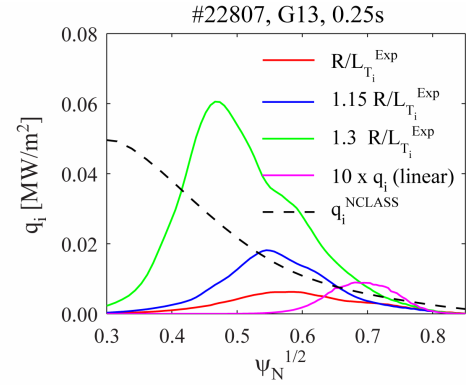

Fig. 6 Ion heat flux q_i from non-linear ORB5 calculations with adiabatic electrons for cases with R/L_{T_i} at the experimental value and increased by a factor 1.15 and 1.3. The ion heat flux from NCLASS and the linear flux are also shown.

4. Summary

Internal transport barriers in the ion thermal and momentum channels form in MAST L-mode discharges in the vicinity of $q_{\min}$. With co-NBI heating, the momentum ITB forms first in a region of negative magnetic shear in the core plasma. Some correlation is found with the strength of the ITB and the passing of $q_{\min}$ through rational values. The strength of the ITB is limited by coupling of MHD modes which reduce the rotation gradient and ultimately, an internal kink mode removes the core flow shear destroying the ITB when q_0 approaches unity. Micro-stability analysis indicates that the negative magnetic shear core region is stable, and flow shear is not required to form the ITB there, while in the outer regions the flow shear is

too weak to stabilize low-*k* ITG modes resulting in anomalous ion transport. At mid-radius shear flow is sufficient to partially stabilise low-*k* TEM modes, leading to incomplete turbulence suppression. With counter-NBI an ion thermal ITB tracks the location of $q_{\min}$ and later bifurcates, an outer ITB following the location of a low order rational surface. The rotation profile is broader than with co-NBI and the thermal transport close to the ion neo-classical level across most of the radius. Measurements of the low-*k* density turbulence in such plasmas using a BES imaging system newly installed on MAST [30] will in future allow direct comparison of results from global turbulence simulations with observations.

This work was funded by the RCUK Energy Programme under grant EP/G003955 and the European Communities under the contract of Association between EURATOM and CCFE. The views and opinions expressed herein do not necessarily reflect those of the European Commission.

[1] R. J. Akers et al., Plasma Phys. and Contr. Fusion, **45** 12A (2003) A175-204.
[2] A. R. Field et al, *'Core heat transport in the MAST spherical tokamak'*, in Proc. 20th Fusion Energy Conf., Vilamoura 2004, IAEA Vienna 2005, EX/P2-11.
[3] R.J. Hawryluk, *'An Empirical Approach to Tokamak Transport", in Physics of Plasmas Close to Thermonuclear Conditions'*, ed. by B. Coppi, et al., (CEC, Brussels, 1980), Vol. 1, pp. 19-46.
[4] E. Joffrin, G. Gorini, C.D. Challis et al., Plas. Phys. Contr. Fus., **44** (2002) 1739.
[5] S. Günter, S. D. Pinches, G. D. Conway et al., 28th EPS Conf. on Plasma Phys, Funchal, 2001, (European Physical Society, 2001), Vol. 25A, p. 49.
[6] X. Garbet, C. Bourdelle, G. T Hoang et al., Phys. Plasmas, **8** (2001) 2793.
[7] F. Romenelli, F. Zonca, Phys. Fluids B, **5** 11 (1993) 4081.
[8] J. F. Drake, Y. T. Lau, P. N. Gudzar et al., Phys. Rev. Lett., **77** (1996) 494.
[9] M. Beer, G. W. Hammett, G. Rewoldt, et al., Phys. Plasmas, **4** (1997) 1792.
[10] C. M. Roach et al., Plasma Physics and Controlled Fusion **51**, 124020 (2009).
[11] S. Saarelma et al., 37th EPS Conf. on Plasma Phys., Dublin, 2010, P1.1061.
[12] M. E. Austin, K. H. Burrell, R. E. Waltz et al., Phys. Plas., **13** (2006) 082502.
[13] H. Y. Yuh, F. M. Levinton, R. E. Bell, et al., Phys. Plasmas, **16** (2009) 056120.
[14] A. R. Field, R. J. Akers, C. Brickley et al., 31st EPS Conf. on Plasma Phys., London, 2004, P4.190.
[15] C. Michael, R. J. Akers, A. R. Field et al., 37th EPS Conf. on Plasma Phys., Dublin, 2010, P1.1067.
[16] I. T. Chapman, M.-D. Hua, S. D. Pinches et al, Nucl. Fus. **50** (2010) 045007.
[17] I. T. Chapman, M.-D. Hua, A. R. Field et al., Plasma Phys. Contr. Fus., **52** (2009) 035009.
[18] R. E. Waltz, G. D. Kerbel, and J. Milovich, Phys. Plasmas **1** 2229 (1994).
[19] M. Kotschenreuther, G. Rewoldt, and W. M. Tang, Comp. Phys. Comm. **88** 128 (1995).
[20] P. J. Catto, M. N. Rosenbluth, and C. S. Liu, Physics of Fluids **16**, 1719 (1973).
[21] A. G. Peeters and C. Angioni, Physics of Plasmas **12**, 072515 (2005).
[22] A. M. Dimits, G. Bateman, and M. A. Beer et al, Phys Plasmas 7, 969 (2000).
[23] J. Kinsey, R. E. Waltz, and J. Candy, Physics of Plasmas 12, 062302 (2005).
[24] M. Barnes et al., http://arxiv.org/abs/1007.3390, submitted to PRL (2010).
[25] E. G. Highcock et al., http://arxiv.org/abs/1008.2305, submitted to PRL (2010).
[26] S. L. Newton, S. C. Cowley, and N. F. Loureiro, submitted to Plas. Phys. and Contr. Fus., http://arxiv.org/abs/1007.0040 (2010).
[27] D. J. Applegate, C. M. Roach, and S. C. Cowley *et al*, Phys. Plasmas **11** 5085 (2004).
[28] S Jolliet et al., Comput. Phys. Commun. **177** (2008) 409.
[29] R. E. Waltz, J. M. Candy and M N Rosenbluth, Phys. Plasmas **9** (2002) 1938.
[30] A. R. Field, D. Dunai, N. J. Conway, S. Zoletnik, J. Sárközi, Rev. Sci. Inst., **80** (2009) 073503.